0026-895X/07/7103-902–911$20.00
MOLECULAR PHARMACOLOGY
Vol. 71, No. 3
29868/3183229
Mol Pharmacol 71:902–911, 2007
Printed in U.S.A.

Neurokinin-3 Receptor-Specific Antagonists Talnetant and Osanetant Show Distinct Mode of Action in Cellular Ca^{2+} Mobilization but Display Similar Binding Kinetics and Identical Mechanism of Binding in Ligand Cross-Competition

Gaochao Tian, Dee Wilkins, and Clay W. Scott

Department of Lead Generation, AstraZeneca Pharmaceuticals, Wilmington, Delaware

Received August 11, 2006; accepted December 15, 2006

ABSTRACT

Talnetant and osanetant, two structurally diverse antagonists of neurokinin-3 receptor (NK_3), displayed distinct modes of action in Ca^{2+} mobilization. Although talnetant showed a normal Schild plot with a slope close to unity and a K_b similar to its K_i value in binding, osanetant presented an aberrant Schild with a steep slope (3.3 $\pm$ 0.5) and a K_b value (12 nM) significantly elevated compared with its K_i value (0.8 nM) in binding. Kinetic binding experiments indicated a simple one-step binding mechanism with relatively fast on- and off-rates for both antagonists, arguing against slow onset of antagonism as the reason for abnormal Schild. This conclusion was supported by prolonged preincubation of antagonist that failed to improve the observed aberrant Schild. In ligand cross-competition binding, both talnetant and osanetant displayed linear reciprocal plots of identical slope when [MePhe^7]neurokinin B (NKB) was used as the other competition partner with ^{125}I-[MePhe^7]NKB as the radioligand, indicating competitive binding of either antagonist with regard to [MePhe^7]NKB. Similar patterns were obtained when talnetant was tested against osanetant, indicating competitive binding between the two antagonists as well. These results were reproduced when [^{3}H]4-quinolinecarboxamide (SB222200), a close derivative of talnetant, was used as the radioligand. Taken together, these data strongly suggest binding of both talnetant and osanetant at the orthosteric binding site with similar kinetic properties and do not support the hypothesis that the aberrant Schild observed in functional assays for osanetant is derived from differences in the mechanism of binding for these NK_3 antagonists.

Neurokinins (NKs) are a family of at least three neuropeptides, substance P, neurokinin A, and neurokinin B (NKB), with each mediating their biological effects through binding to a preferred G-protein-coupled receptor termed NK_1, NK_2, or NK_3, respectively (Holmes et al., 2003; Almeida et al., 2004; Gerspacher, 2005; Spooren et al., 2005). All three NK receptors are expressed in regions of the central nervous system that are related to emotion and cognition (i.e., amygdala and hippocampus) and have been linked to various degrees in psychiatric disorders (Albert, 2004). Although early drug discovery efforts in this area were mainly focused on NK_1, increased attention has been given to NK_2 and NK_3. Intense drug discovery activities have led to the characterization of many small-molecule antagonists and clinical trials of several for each receptor, with some showing encouraging clinical results (Holmes et al., 2003; Almeida et al., 2004; Gerspacher, 2005; Spooren et al., 2005). Two NK_3 receptor-specific small-molecule antagonists, osanetant and talnetant (Fig. 1), have advanced to phase II clinical trials for schizophrenia, displaying promising antipsychotic effects and good drug tolerability (Almeida et al., 2004; Kronenberg et al., 2005; Spooren et al., 2005).

The pharmacological properties of osanetant and talnetant have been extensively documented. Both antagonists potently and selectively inhibit the binding of ^{125}I-[MePhe^7]NKB and function of NK_3 in a number of cellular and tissue assays (Almeida et al., 2004). However, the mechanisms of action for these two compounds seem to be different. In Ca^{2+}-mobilization assays, talnetant unequivocally demonstrates reversible and time-independent competitive antagonism (Sarau et al., 1997; Giardina et al., 1999). Given its surmountable nature displayed in both binding and tissue functional assays (Sarau et al., 1997), this competitive antagonism profile supports the notion that binding of talnetant occurs at the orthosteric site. The mechanism of action by osanetant has been controversial. It displays a linear Schild plot with a slope of unity in senktide [(succinyl-

Article, publication date, and citation information can be found at http://molpharm.aspetjournals.org.
doi:10.1124/mol.106.029868.

ABBREVIATIONS: NK, neurokinin; NKB, neurokinin B; BSA, bovine serum albumin; D_2, dopamine receptor 2; SPA, scintillation proximity assay; CHO, Chinese hamster ovary.

[Asp^9,MePhe^8])-SP(6–13)]-induced contraction of rabbit iris sphincter muscles, indicating competitive antagonism, but this competitive pattern does not hold when other agonists, such as [MePhe^7]NKB or [Pro^7]NKB, are used in the same procedure (Giardina et al., 1999). Osanetant also shows a linear Schild in [MePhe^7]NKB-induced contraction of guinea pig ileum (Medhurst et al., 1997), albeit the effect seems to be time-dependent and irreversible (Emonds-Alt et al., 1995), contradicting the conclusion of competitive binding that would be otherwise implied by the linear Schild (Nguyen-Le et al., 1996). Adding to the confusion, insurmountable antagonism is observed for osanetant in senktide-induced inositol phosphate turnover in guinea pig ileum with a partial reduction in maximal agonist response (Beaujouan et al., 1997), a result more consistent with noncompetitive antagonism. So GE Healthcare far, no mechanistic studies have been performed for osanetant in the Ca^{2+} mobilization assay, in which talnetant displays competitive antagonism (Giardina et al., 1999). The relatively well-defined competitive antagonism for talnetant and the controversy in the mechanism of action for osanetant, together with the fact that the structures for these two compounds are distinct (Fig. 1), raise the question of how the two antagonists produce different functional effects if osanetant and talnetant exert their pharmacological effects through interaction with NK_3 at the same site on the receptor and if they indeed occupy the same binding site on the receptor.

In the current investigation, the mode of action for osanetant in the Ca^{2+} mobilization assay was investigated, and the result was compared with that for talnetant. To provide clues as to whether the antagonists bind at different sites on NK_3, the patterns of competition binding for both compounds with orthosteric ligand and one another were studied using ligand cross-competition, a novel mechanistic probe to study receptor antagonists. Kinetics of binding for both of the NK_3 antagonists were also measured to provide insights into the time-dependence and reversibility of the binding reactions.

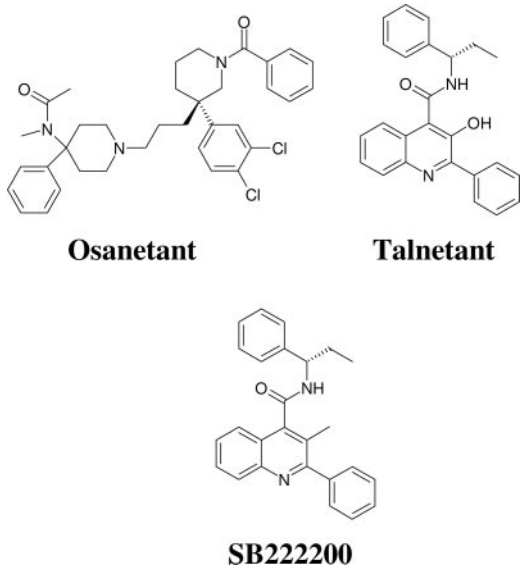

Fig. 1. Chemical structures of talnetant, osanetant, and SB222200. Talnetant, also named SB223412, is (*S*)-(−)-*N*-(α-ethylbenzyl)-3-hydroxy-2-phenylquinoline-4-carboxamide. Osanetant (SR142801), is (*S*)-(+)-*N*-{[3-[1-benzoyl-3-(3,4-dichlorophenyl)piperidin-3-yl]prop-1-yl}-4-phenylpiperidin-4-yl}-*N*-methylacetamine. SB222200 is (*S*)-(−)-*N*-(α-ethylbenzyl)-3-methyl-2-phenylquinoline-4-carboxamide and is identical with talnetant except that the 3-hydroxyl of the phenylquinoline is replaced with a methyl group.

Materials and Methods

Materials. Tris-HCl, HEPES, $MnCl_2 \cdot 4H_2O$, probenecid, and BSA were purchased from Sigma (St. Louis, MO). [MePhe^7]NKB and senktide were from Bachem (Bubendorf, Switzerland). Fluo-4/acetoxymethyl ester was from Invitrogen (Carlsbad, CA). UltraCulture, Hanks' balanced salt solution, and L-glutamine were from Cambrex Bio Science Walkersville, Inc. (Walkersville, MD). Poly(D-lysine)-coated 384-well plates were from BD Biosciences (San Jose, CA). Polyvinyltoluene-wheat germ agglutinin scintillation proximity assay (SPA) beads were from GE Healthcare (Little Chalfont, Buckinghamshire, UK). Unifilter GF/C 96-well plates and ^{125}I-[MePhe^7]NKB were from PerkinElmer Life and Analytical Sciences (Boston, MA). [^{3}H]SB222200 and [^{3}H]SR142801 ([^{3}H]osanetant) were obtained from American Radiolabeled Chemicals (St. Louis, MO). Membranes from CHO cells overexpressing recombinant human NK_3 were prepared by Applied Cell Services (Rockville, MD). Thiorpan, talnetant, osanetant, and SB222200 were prepared in the Department of Medicinal Chemistry, AstraZeneca Pharmaceuticals (Wilmington, DE).

Radioligand Filter Binding Assays. Filter radioligand binding assays, performed in 96-well polypropylene U-bottomed plates with a final assay volume of 200 μl, were run in 50 mM Tris-HCl, pH 7.4, containing 4 mM $MnCl_2$ (powder added fresh before assay), 1 mg/ml BSA, 10 μM thiorphan (3-mercapto-2-benzylpropanoylglycine), 1% dimethyl sulfoxide, and membranes of CHO cells overexpressing human recombinant NK_3 receptor at a final total membrane protein concentration of 10 μg/ml. Assay solutions were incubated at room temperature (22°C) on a plate shaker for 1 h unless specified otherwise, followed by filtration through a 96-well filter-bottomed plate (Unifilter GF/C; PerkinElmer Life and Analytical Sciences) pretreated with 0.5% BSA to capture the radioligand-receptor binding complex. The captured binding complex was then washed with 4× 300 μl/well wash buffer (20 mM Tris-HCl, pH 7.0, containing 0.2 mg/ml BSA) to remove unbound radioligand. After the filter-bottomed plates were dried in air for >4 h, 40 μl/well scintillant was added, and the plates were then sealed and read on a TopCount scintillation counter (PerkinElmer Life and Analytical Sciences) to quantify bound radioligand.

For radioligand saturation binding, the isotope concentration was varied between 0 and 20 nM for [^{3}H]SB222200 and between 0 and 1.25 nM for ^{125}I-[MePhe^7]NKB. A binding assay in the absence of receptor was also performed for each isotope concentration used to provide a background control for that particular isotope concentration. For competition binding, in assays with [^{3}H]SB222200 or [^{3}H]SR142801 as the radioligand, the isotope was added at a final concentration of 1 nM unless specified otherwise. For assays using ^{125}I-[MePhe^7]NKB, the final isotope concentration was set at 0.1 nM. In competition binding, 2 μl of dimethyl sulfoxide solution of a test compound (simple competition binding) or two compounds (ligand cross-competition, see below) at specified final concentrations was first added to assay plates followed by the addition of 198 μl of buffer containing all other assay components to initiate ligand competition. In studying kinetics of radioligand binding for determining association rate constants, radioligand and receptor were mixed at varied times between 0 and 120 min before filtration, whereas in measuring dissociation rate constants, radioligand and receptor were mixed and incubated for >20 min before a 10-fold dilution into a buffer solution containing the homologous nonradioactive ligand at a concentration >10,000 × K_d value.

Scintillation Proximity Assay. SPAs, run only with ^{125}I-[MePhe^7]NKB as the radioligand, were performed under the same assay conditions as in the filter-binding assay, except that 1.5 mg/ml SPA beads were included. The beads were presoaked in the assay buffer for ~10 min before the addition of other assay components.

Ca^{2+} Mobilization Assay. Stably transfected CHO cells overexpressing human recombinant NK_3 were plated into poly(D-lysine) coated 384-well plates at a concentration of 10,000 cells/well in UltraCulture media (Cambrex Bio Science Walkersville, Inc.) with 2 mM L-glutamine. The cells were incubated overnight at 37°C with 5% CO_2. The next day, cell media were aspirated from the cell plate, and 25 μl of Fluo-4/acetoxymethyl ester solution at a final concentration of 4.4 μM Fluo-4 in assay buffer (15 mM HEPES, pH 7.4, Hanks' balanced salt solution, and 2.5 mM probenecid) was added to each well. After being incubated at 37°C for 1 h, the cell plate was washed twice to remove excess dye, leaving behind fresh assay buffer. After the addition of antagonist at various concentrations to the cell plate and preincubation with cells at room temperature (22°C) for 10 min, senktide was added by the fluorometric imaging plate reader instrument. Immediately thereafter, measurements of the fluorescent intensity were taken every second for 1 min, with the laser set at 0.60 W and the exposure length at 0.40.

Theory of Ligand Cross-Competition. Inhibitor cross-competition has been used in determining the mode of action between enzyme inhibitors (Tian et al., 2003; Knappenberger et al., 2004). However, there have been no reports describing its application in receptor binding. Analogous to an enzyme assay, ligand cross-competition would measure effects on binding of radioligand (A) (i.e., radiolabeled agonist), by two receptor ligands (I_1 and I_2) (i.e., antagonists) present in the assay simultaneously. In the current study, the ternary complex model with a single orthosteric binding site was used as the basis for developing the theory for ligand cross-competition, assuming that each of the two competition partners binds to receptor (R) noncompetitively with regard to one another and to the orthosteric radioligand as shown in Scheme 1. In this scheme, K_d, $K_{i(1)}$, and $K_{i(2)}$ are constants for dissociation of binary complexes RA, RI_1, and RI_2, respectively, α, β, and γ are cooperativity factors for the formation of ternary complexes RAI_1, RAI_2, and RI_1I_2, respectively, and δ is the cooperativity factor responsible for the formation of the tertiary complex RAI_1I_2. The size of each cooperativity factor determines the apparent mode of action of the antagonist for a particular binding step with which the cooperativity factor is associated. The greater the size the cooperativity factor is, the more competitive the antagonist would be with regard to the other ligand involved in that particular binding step. For example, two ligands are strictly competitive if the cooperativity factor is approaching infinity but purely noncompetitive if the cooperativity factor is unity. Therefore, to determine the mode of action of an antagonist is to assess the size of the cooperativity factors associated with its binding reactions. This requires an analytical description of the system. For the system shown in Scheme 1, the solution is given by the following equation (see *Appendix*):

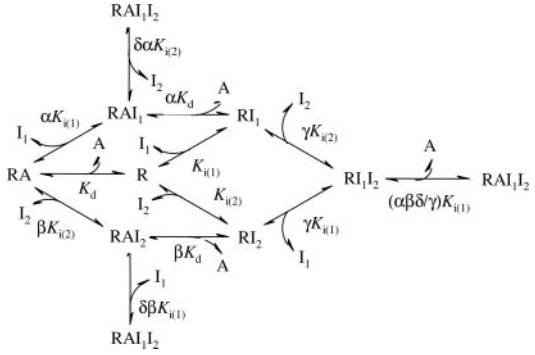

Scheme 1. Model of ligand cross-competition between antagonist ligands. In this ternary complex model with a single orthosteric binding site, two antagonist ligands I_1 and I_2 compete for binding sites on receptor (R), with each binding to R noncompetitively with regard to one another and to the orthosteric ligand (A).

$$B = \frac{B_{max}\dfrac{[A]}{K_d+[A]}\left(1+\dfrac{[I_1]}{\alpha K_{i(1)}}+\dfrac{[I_2]}{\beta K_{i(2)}}+\dfrac{[I_1][I_2]}{\alpha\beta\delta K_{i(1)}K_{i(2)}}\right)}{1+\left(\dfrac{\alpha K_d+[A]}{K_d+[A]}\right)\dfrac{[I_1]}{\alpha K_{i(1)}}+\left(\dfrac{\beta K_d+[A]}{K_d+[A]}\right)\dfrac{[I_2]}{\beta K_{i(2)}}+\left(\dfrac{(\alpha\beta\delta/\gamma)K_d+[A]}{K_d+[A]}\right)\dfrac{[I_1][I_2]}{\alpha\beta\delta K_{i(1)}K_{i(2)}}} \quad (1)$$

Derived assuming noncompetitive binding for all the binding equilibriums involved, eq. 1 is the most general solution for describing ligand cross-competition and is a relatively complicated function to use. For certain cases, it can be reduced. If the mode of action of one antagonist (i.e., I_1) with regard to the orthosteric ligand is competitive (α, $\delta \to \infty$), the solution becomes

$$B = \frac{B_{max}\dfrac{[A]}{K_d+[A]}\left(1+\dfrac{[I_2]}{\beta K_{i(2)}}\right)}{1+\left(\dfrac{K_d}{K_d+[A]}\right)\dfrac{[I_1]}{K_{i(1)}}+\left(\dfrac{\beta K_d+[A]}{K_d+[A]}\right)\dfrac{[I_2]}{\beta K_{i(2)}}+\left(\dfrac{K_d}{K_d+[A]}\right)\dfrac{[I_1][I_2]}{\gamma K_{i(1)}K_{i(2)}}} \quad (2)$$

In a special case in which the nonradioactive homologous ligand is one (I_1) of the competition partners, the radioligand (A) and the homologous ligand (I_1) would be indistinguishable mechanistically and must be competitive (α, $\delta \to \infty$). Their thermodynamic properties are also likely to be very close ($\beta \cong \gamma$), if not identical. As a result, the solution for such a "homologous" ligand cross-competition can be approximated by eq. 3:

$$B = \frac{B_{max}\dfrac{[A]}{K_d+[A]}\left(1+\dfrac{[I_2]}{\gamma K_{i(2)}}\right)}{1+\left(\dfrac{K_d}{K_d+[A]}\right)\dfrac{[I_1]}{K_{i(1)}}+\left(\dfrac{\gamma K_d+[A]}{K_d+[A]}\right)\dfrac{[I_2]}{\gamma K_{i(2)}}+\left(\dfrac{K_d}{K_d+[A]}\right)\dfrac{[I_1][I_2]}{\gamma K_{i(1)}K_{i(2)}}} \quad (3)$$

If both I_1 and I_2, are competitive against A (α, β, $\delta \to \infty$), the solution is further reduced to

$$B = \frac{B_{max}\dfrac{[A]}{K_d+[A]}}{1+\left(\dfrac{K_d}{K_d+[A]}\right)\dfrac{[I_1]}{K_{i(1)}}+\left(\dfrac{K_d}{K_d+[A]}\right)\dfrac{[I_2]}{K_{i(2)}}+\left(\dfrac{K_d}{K_d+[A]}\right)\dfrac{[I_1][I_2]}{\gamma K_{i(1)}K_{i(2)}}} \quad (4)$$

Finally, if both I_1 and I_2, are competitive against A and also competitive against one another (α, β, γ, $\delta \to \infty$), the system is the simplest for ligand cross-competition, with the solution given by eq. 5:

$$B = \frac{B_{max}\dfrac{[A]}{K_d+[A]}}{1+\left(\dfrac{K_d}{K_d+[A]}\right)\dfrac{[I_1]}{K_{i(1)}}+\left(\dfrac{K_d}{K_d+[A]}\right)\dfrac{[I_2]}{K_{i(2)}}} \quad (5)$$

These various scenarios may be distinguished by analyzing data according to eqs. 1 to 5. In the case where both competition partners are competitive with the orthosteric ligand, whether the two competition partners are competitive with one another may also be determined graphically by reciprocal plots. For example, the reciprocal of eq. 5 describing competitive binding is given by

$$\frac{1}{B} = \frac{K_d+[A]}{B_{max}[A]}+\left(\frac{K_d}{B_{max}[A]K_{i(2)}}\right)[I_2]+\left(\frac{K_d}{B_{max}[A]K_{i(1)}}\right)[I_1] \quad (6)$$

which indicates that the plot of $1/B$ versus $[I_1]$ is linear and $[I_2]$ will affect the intercept but not the slope. Therefore, plotting $1/B$ versus $[I_1]$ at different values of $[I_2]$ would yield a group of linear parallel

lines (Fig. 2A). In comparison, the reciprocal of eq. 4 for noncompetitive cross-competition is given by eq. 7:

$$\frac{1}{B} = \frac{K_d + [A]}{B_{max}[A]} + \left(\frac{K_d}{B_{max}[A]K_{i(2)}}\right)[I_2] + \frac{K_d}{B_{max}[A]K_{i(1)}}\left(1 + \frac{[I_2]}{\gamma K_{i(2)}}\right)[I_1] \quad (7)$$

from which a group of linear lines with different slopes, as well as different intercepts, is predicted (Fig. 2B).

Data Analysis. Data from radioligand (A) saturation binding after subtracting the values from control wells (in the absence of receptor) were first transformed into molar concentrations of bound species (B) using the specific activity of the isotope and estimated counting efficiency. These values were further analyzed according to the following equation to determine B_{max} and K_d:

$$B = \frac{B_{max}[A]}{K_d + [A]} \quad (8)$$

IC_{50} values from competition binding by antagonist (I) were determined by subtracting the background counts (wells with 100 nM [MePhe^7]NKB), determining the percentage of bound ($\%B$) relative to the maximum wells (those in the absence of antagonist), and then fitting $\%B$ as a function of antagonist concentration according to eq. 9:

$$\%B = 100\left(1 - \frac{[I]}{IC_{50} + [I]}\right) \quad (9)$$

Dose-response from Ca^{2+} mobilization assays generated in the presence of antagonist were fit to the following equation to determine apparent EC_{50} value:

$$\%E = 100\left(\frac{[A]}{EC_{50} + [A]}\right) \quad (10)$$

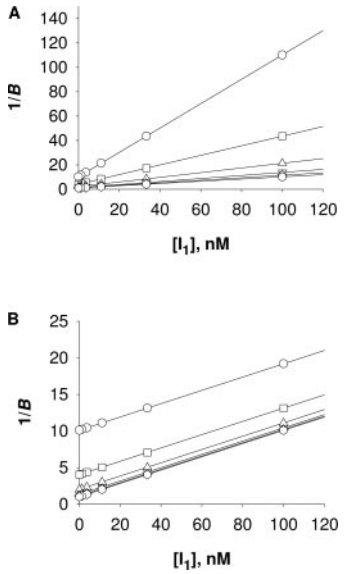

Fig. 2. Theoretical reciprocal plots for data from ligand cross-competition. A, noncompetitive cross-competition between two antagonists I_1 and I_2 with $[I_2]$ set at 0 (hexagon), 12.4 (◇), 37.0 (▽), 111 (△), 333 (□), and 1000 (○) nM. The lines were calculated using eq. 8 normalized by multiplying both sides of the equation with $B_{max}[A]/(K_d + [A])$, with K_d = 2 nM, [A] = 0.2 nM, $K_{i(1)}$ = 10 nM, $K_{i(2)}$ = 100 nM, and γ = 1. B, competitive cross-competition between two antagonists I_1 and I_2 with $[I_2]$ set at 0 (hexagon), 12.4 (◇), 37.0 (▽), 111 (△), 333 (□), and 1000 (○) nM. The lines were calculated using eq. 7 normalized by multiplying both sides of the equation with $B_{max}[A]/(K_d + [A])$ with K_d = 2 nM, [A] = 0.2 nM, $K_{i(1)}$ = 10 nM, and $K_{i(2)}$ = 100 nM.

where A is agonist. The subsequent Schild analysis was performed by fitting the dose ratio, defined as $EC_{50[I]}/EC_{50[I]=0}$, as a function of [I] according to eq. 11:

$$\log(dr - 1) = -s\log[I] + i \quad (11)$$

from which pA_2 was calculated as i/s.

Assuming a simple, one-step reversible binding mechanism and the presence of ligand in excess of receptor ([A] ≫ [R]), data (B, bound radioligand) from association kinetic radioligand binding at various times, t, were fit to the following equation:

$$B = (B_0 - b)(1 - e^{-(1/\tau)t}) + b \quad (12)$$

where B_0 is bound ligand at equilibrium, b is background binding, t is time, and τ is the relaxation time for reaching equilibrium, which is given by

$$1/\tau = k_{on}[A] + k_{off} \quad (13)$$

with k_{on} and k_{off} designated, respectively, as the rate constants for the forward and backward reactions. Data from radioligand dissociation kinetics were fit to the following equation:

$$B = (B_0 - b)e^{-(1/\tau)t} + b \quad (14)$$

Here the apparent first-order rate constant $k_{on}[A]$ is functionally insignificant given the dissociation kinetics was carried out by diluting radioligand-receptor into a solution containing >1000-fold excess nonradioactive homologous ligand, and therefore,

$$1/\tau \cong k_{off} \quad (15)$$

Data from ligand cross-competition with the nonradioactive homologous ligand as one of the competition partners were analyzed by nonlinear squares analysis using eq. 3. Data from other ligand cross-competition assays were analyzed by nonlinear squares analysis using eqs. 1, 2, 4, or 5. Linear parallel reciprocal plots were generated according to eq. 6 using parameters obtained from fitting data to eq. 5.

To determine whether temporal effects played a role in observed Schild slope from the Ca^{2+} mobilization assay, the following nonequilibrium Schild equation (Kenakin, 1980) was used in data analysis:

$$\log(dr_t - 1) = \log[B] - \log K_b + \log\frac{1 - e^{-k_2(1 + [B]/K_b)t}}{1 + ([B]/K_b)e^{-k_2(1 + [B]/K_b)t}} \quad (16)$$

where dr_t is dose ratio at time t, B is antagonist, K_b is dissociation constant for B, and k_2 is dissociation rate constant.

Results

Talnetant and Osanetant Show Different Modes of Action in Intracellular Ca^{2+} Mobilization. Although reversible, time-independent competitive antagonism for talnetant is observed using Ca^{2+} mobilization (Giardina et al., 1999), no comparable data with osanetant has been published. As such, intracellular Ca^{2+} mobilization was first used to determine whether osanetant would exert its functional effect in a similar fashion as talnetant. These experiments were performed by incubating antagonist for 10 min with CHO cells overexpressing NK_3 and preloaded with the Ca^{2+}-detecting dye Fluo-4, followed by the addition of agonist (senktide, EC_{50} = 0.77 ± 0.26 nM) and reading of fluorescence immediately thereafter. Dose-response at various concentrations of antagonist was analyzed according to eq. 10 to determine apparent EC_{50}, which was then plotted against [I] (eq. 11) to determine the Schild slope and pA_2.

As shown in Fig. 3, talnetant displayed a linear Schild plot

with slope close to unity (1.3 ± 0.2; Table 1) and a pA_2 of 8.82. This value translates into an apparent K_b of 1.5 nM, a value of the same magnitude as the K_i (5 nM, data not shown) as determined in radioligand competition binding. These results are consistent with data from previous reports (Sarau et al., 1997; Giardina et al., 1999) suggesting competitive binding of talnetant with regard to the orthosteric ligand. In contrast, osanetant showed a steep Schild (○, Fig. 4B) with a slope far from unity (3.3 ± 0.3) and a pA_2 of 7.94 (Table 1), which is equivalent to an apparent K_b value of 12 nM, a value significantly greater than its IC_{50} (0.8 nM; data not shown) as determined in radioligand competition binding. The discrepancy between binding and functional potencies, and the observed abnormal Schild, suggested a more complicated mode of action for osanetant.

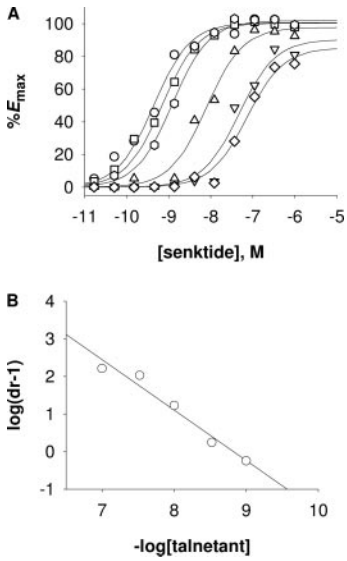

Fig. 3. Schild analysis of talnetant in the Ca^{2+} mobilization assay. The Ca^{2+} mobilization assay was carried out with a preincubation of talnetant at 0 (○), 1 (□), 3 (hexagon), 10 (△), 30 (▽), and 100 (◇) nM for 10 min and fluorescence as the function of senktide concentration was quantified as the percentage of maximum effect (A). The dose-ratio as a function of talnetant concentration (B) was then plotted to yield a slope of 1.3 ± 0.2 and pA_2 of 8.82.

TABLE 1

Summary of Schild constants for talnetant and osanetant in Ca^{2+} mobilization assay

Assays were carried out by incubating antagonist at various concentrations with CHO cells overexpressing human recombinant NK_3 for 10 min before the addition of senktide. The dose-response curves at various senktide concentrations were fit to eq. 10 to determine apparent EC_{50} values at each concentration of antagonist, and the dose ratio was then plotted against [I] according to eq. 11 to determine Schild slope and pA_2.

Compound	Schild Slope	pA_2	K_b	t^a
			nM	*min*
Talnetant[b]	1.3 ± 0.2	8.82	1.5	10
Talnetant[c]	0.90		3.0	
SB222200[b]	0.92		3.3	10
Osanetant[b]	3.3 ± 0.3	7.94	12	10
	3.1 ± 0.3	8.03	9	30
	2.9 ± 0.3	8.02	10	55

[a] Preincubation time.
[b] From this work with K_b values calculated from pA_2.
[c] From NKB-induced Ca^{2+} mobilization in human embryonic kidney 293 cells overexpressing human recombinant NK_3 with K_b values calculated by averaging values estimated from displacement of agonist dose-response curve at various concentrations of antagonist (Sarau et al., 2000).

Osanetant Shares Similar Binding Kinetics with SB22220 and Talnetant. To determine association kinetics, [^{3}H]osanetant was mixed with receptor for various times followed by filtration through a filter plate to quantify bound radiolabel. For dissociation kinetics, receptor and [^{3}H]osanetant were preincubated for 20 min, diluted into a large excess of unlabeled ligand, and the amount of radioligand remaining bound at various times was followed by filtration. As shown in Fig. 5A, both association and dissociation of radiolabeled osanetant seemed to follow a monotonic process, indicating a simple one-step binding mechanism. Complete dissociation of bound radioligand occurred after the 20-min preincubation, indicating reversible binding under these conditions. To determine whether irreversible binding would only occur after a longer time of association, the dissociation kinetics were performed with a longer preincubation. As shown in Fig. 5B, preincubation at up to 2 h did not appreciably perturb the dissociation kinetics of osanetant, ruling out slow onset of irreversible binding. The apparent first-order rate constant k_{on}[A] and k_{on} and k_{off} (Table 2) were then obtained by analyzing data according to eqs. 12 to 15 assuming a one-step reversible binding. Similar kinetic results were obtained with ^{125}I-[MePhe^7]NKB and [^{3}H]SB222200 (Fig. 5A and Table 2), a close derivative of

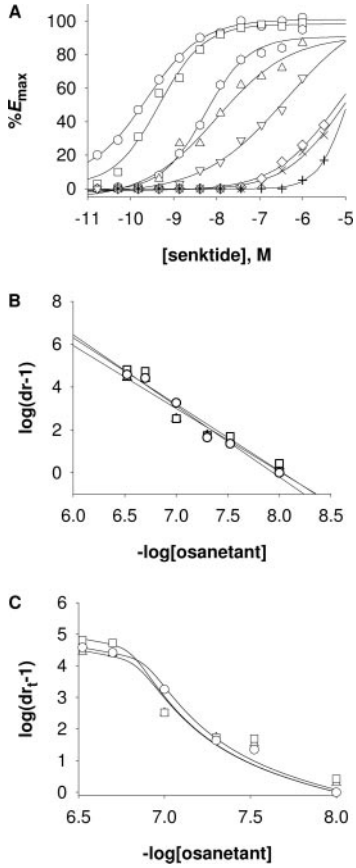

Fig. 4. Schild analysis of osanetant in the Ca^{2+} mobilization assay. The Ca^{2+} mobilization assay was carried out with a preincubation of osanetant at 0 (○), 3 (□), 10 (hexagon), 30 (△), 100 (▽), and 300 (◇) nM for 10 min and fluorescence as the function of senktide concentration was quantified as the percentage of maximum effect (A). The dose-ratio as a function of osanetant concentration with preincubation of antagonist for 10 (○), 30 (□), and 55 (△) min (B). The dose-ratio versus [osanetant] were fit to the temporal equation for data obtained with preincubation of antagonist for 10 (○), 30 (□), and 55 (△) min (C).

talnetant (Fig. 1). The dissociation kinetics for talnetant was assessed by a "hot-chase" isotope exchange procedure in which preformed bound species were diluted into assay buffer containing ^{125}I-[MePhe^7]NKB, allowing binding of the radiolabel to the receptor as a result of dissociation of talnetant (Fig. 5C). The apparent rate constant for association of ^{125}I-[MePhe^7]NKB was then taken as the apparent dissociation constant for talnetant. The true dissociation constant for talnetant might have been underestimated by this approach (i.e., limited by the rate of radiolabel association of 0.16 min^{-1}; Table 2) for this value was comparable with the apparent dissociation rate constant of talnetant so determined (0.13 min^{-1}, Table 2). As shown in Table 2, the rate constant for association, k_{on}, for osanetant (0.23 nM^{-1} · min^{-1}) is very close to that (0.13 nM^{-1} · min^{-1}) determined for SB222200, a close derivative of talnetant (Table 1). The k_{off} values (0.03 min^{-1}, osanetant; 0.07 min^{-1}, SB222200; 0.13 min^{-1}, talnetant; Table 2) are also similar for the three antagonists. These results indicate that the kinetic profile of osanetant is similar to those of talnetant and its derivative SB222200.

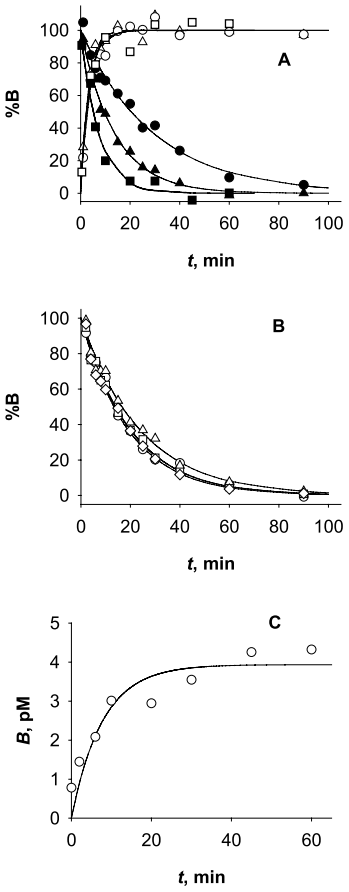

Fig. 5. Binding kinetics of [MePhe^7]NKB, SB222200, osanetant, and talnetant. Binding assays (A) were used to measure the association (open symbols) and dissociation (closed symbols) of [^{3}H]osanetant (circles), [^{3}H]SB222200 (triangles), and ^{125}I-[MePhe^7]NKB (squares) as a function of time. The data were fit to eqs. 11 and 13, respectively, to determine the relaxation times for the association and dissociation kinetics. Dissociation kinetics for osanetant (B) were measured after preincubating [^{3}H]osanetant with receptor for 30 (○), 60 (□), 90 (△), and 120 min (◇). Dissociation kinetics for talnetant was assessed by a "hot-chase" procedure (C) in which the antagonist was preincubated with receptor for 20 min followed by dilution of mixture into an assay buffer containing ^{125}I-[MePhe^7]NKB.

TABLE 2

Summary of parameters for kinetic binding of various ligands to NK_3

All of the values were obtained in 50 mM Tris-HCl, pH 7.4, at 22°C. Radiolabeled osanetant, SB222200, and [MePhe^7]NKB were used in filter binding assays to quantify association and dissociation binding kinetics. The apparent first-order rate constant for association k_{on}[A], k_{on}, and k_{off} were obtained by fitting data to eqs. 12 to 14. The k_{off} value for talnetant was determined using a hot-chase procedure with ^{125}I-[MePhe^7]NKB as discussed under *Materials and Methods*. The K_d values were taken as the ratio of k_{off}/k_{on}.

Compound	k_{on}[A]	k_{on}	k_{off}	K_d
	min^{-1}	*min^{-1}nM^{-1}*	*min^{-1}*	*nM*
Osanetant	0.23	0.23	0.03 ± 0.01	0.15
SB222200	0.26	0.13	0.07 ± 0.01	0.56
[MePhe^7]NKB	0.16	1.55	0.14 ± 0.02	0.09
Talnetant	N.D.	N.D.	>0.13 ± 0.04	N.D.

Not determined.

Prolonged Preincubation of Osanetant Does Not Improve the Aberrant Schild in the Ca^{2+} Mobilization Assay. Schild analysis of osanetant in the Ca^{2+} mobilization assay was repeated with longer preincubation times to investigate further the question of inadequate antagonist-receptor interaction as the reason for the aberrant Schild slope observed with osanetant (3.3, Table 1). As shown in Fig. 4B, the Schild plots at 30 (□) and 50 (△) min of preincubation times were almost identical with the one obtained with the 10 min preincubation (○), with the slopes being 3.1 and 2.9 (Table 1), respectively, for plots obtained at the 30- and 55-min preincubation. These values were comparable with the slope of 3.3 obtained with the 10-min preincubation. Likewise, the pA_2 values were 8.0 in both cases, a value not significantly different from 7.9 (Table 1) observed with the 10-min preincubation. These data indicate that the aberrant Schild observed with the 10-min preincubation cannot be improved by extending the preincubation time.

Data Analysis Using the Temporal Schild Equation Yields Very Small K_b and k_2 Values. The data of dose ratio against osanetant concentration from the Ca^{2+} mobilization assay could also fit reasonably well according to the temporal equation (eq. 16) for Schild (Kenakin, 1980), as shown in Fig. 4C. However, this analysis yielded very small values for K_b (8, 4, and 10 pM, respectively, for 10-, 30-, or 55-min preincubation) and k_2 (6.3×10^{-5}, 9.8×10^{-6}, and 1.3×10^{-5} min^{-1}, respectively, for 10-, 30-, or 55-min preincubation), making it difficult to reconcile with values determined in direct kinetic (k_{off} of 3.0×10^{-2} min^{-1}, Table 2), competition ligand binding (IC_{50} = 0.8 nM; data not shown), and ligand cross-competition (K_i = 0.2–0.6 nM; Table 3) studies.

Talnetant and Osanetant Bind Competitively with Regard to [MePhe^7]NKB and to Each Other. Ligand cross-competition examines how the copresence of two ligands (i.e., two antagonists) would affect the binding of the orthosteric ligand (i.e., the agonist). This method (see Theory of Ligand Cross-Competition), in principle, allows the prediction of whether the two cross-competition partners are competitive or noncompetitive with regard to one another. In practice, varying concentrations of two ligands ([I_1] and [I_2]) are insufficient to solve simultaneously four cooperativity factors (α, β, γ, and δ) according to eq. 1. It is more practical if the mechanism of binding for each antagonist with regard to the orthosteric ligand has already been solved, reducing the total number of cooperativity factors that needs to be estimated from four to two (γ and δ). This can be achieved by

ligand cross-competition by first using the homologous ligand with each antagonist and applying eq. 4, where only one cooperativity factor (γ) needs to be calculated.

SPA binding using ^{125}I-[MePhe^7]NKB as the radioligand was used first for ligand cross-competition studies. Saturation binding yielded a K_d value of 0.9 nM (data not shown) for ^{125}I-[MePhe^7]NKB. Cross-competition with the homologous ligand [MePhe^7]NKB for osanetant and then with talnetant was subsequently carried out using 0.1 nM ^{125}I-[MePhe^7]NKB. Fitting data according to eq. 3 yielded a large γ value for the homologous cross-competition with either osanetant or talnetant (Table 3), and the corresponding reciprocal plots were linear and parallel (Figs. 6, A and B), indicating that each antagonist binds to NK_3 competitively with regard to the homologous ligand [MePhe^7]NKB. Subsequent heterologous ligand cross-competition studies between osanetant and talnetant, assuming competitive binding of each with regard to [MePhe^7]NKB (eq. 4), also produced a large γ value (Table 3) and linear parallel reciprocals (Fig. 6C), indicating competitive binding between the two antagonists as well. Similar results (large γ values, Table 3, and linear parallel reciprocals, Fig. 7) were obtained using [^{3}H]SB222200 as the radioligand for both homologous and heterologous ligand cross-competition. The K_i values for [MePhe^7]NKB, talnetant, osanetant, and SB222200 determined from these ligand cross-competition experiments were all similar to their respective K_i values as measured independently in radioligand competition binding assays (data not shown). Taken together, these data strongly suggest that osanetant and talnetant bind at the same pocket within the orthosteric binding site on NK_3, resulting in the observed competitive binding patterns for osanetant and talnetant with regard to the orthosteric ligand and between themselves.

Discussion

The primary objective of the current study was to investigate and clarify differences in the mode of action between talnetant and osanetant, two well-documented small-molecule NK_3 antagonists of distinct chemical structures (Fig. 1). The mode of action of talnetant is relatively well understood, documented in literature as a time-independent, reversible, competitive, and orthosteric binding antagonist (Sarau et al., 1997; Giardina et al., 1999). The mode of action for osanetant has also been described in several functional assays, including inositol phosphate turnover, muscle contraction in guinea pig ileum, and contraction of the rabbit iris sphincter muscle, however, with different assays yielding results suggesting different mode of action (Emonds-Alt et al., 1995; Nguyen-Le et al., 1996; Beaujouan et al., 1997; Medhurst et al., 1997). In the current investigation, talnetant showed a normal, linear Schild plot in the Ca^{2+} mobilization assay (Fig. 3) whereas osanetant displayed an aberrant Schild with a slope as much as 3.3 (Fig. 4), reinforcing the findings on these NK_3 antagonists documented previously.

What causes osanetant to behave functionally differently from talnetant? To address this question, several possibilities may be considered. First of all, the observed steep slope in Schild analysis of osanetant in Ca^{2+} mobilization (Fig. 4) can be explained if equilibrium is not attained at lower concentrations of antagonist. As such, at low concentrations of antagonist, the time to reach equilibrium would be long, resulting in partial binding and, therefore, underestimated antagonist potency, skewing the Schild slope upward (Kenakin, 1980; Lutz and Kenakin, 1999). Consistent with this hypothesis, several reports have demonstrated the slow onset of and long-lasting functional effects by osanetant (Nguyen-Le et al., 1996; Beaujouan et al., 1997), raising the possibility that the binding kinetics for osanetant might indeed be quite different from talnetant, involving slow on- and off-rates or functionally irreversible binding steps.

To investigate this possibility, kinetic binding assays were performed with osanetant, and the results were compared with those obtained with talnetant and its close derivative SB222200, which has also been demonstrated to show normal Schild behavior as talnetant in Ca^{2+} mobilization (Sarau et al., 2000). As shown in Table 2, the kinetic parameters displayed by osanetant are quite similar to those obtained for talnetant (Table 2). In particular, the k_{on} of 0.23 $nM^{-1} \cdot min^{-1}$ (Table 2) for osanetant would translate into a $t_{1/2}$ of only 0.3 min for antagonist binding even at the lowest concentration (10 nM) of osanetant used in the Schild analysis. That such a short half-life is sufficient for equilibration with a 10-min preincubation in Ca^{2+} mobilization, together with the fact that the kinetic profiles for talnetant and osanetant are very similar, does not support the hypothesis of slow onset of binding as the cause for the observed aberrant Schild for osanetant.

However, it can be argued that the kinetic properties displayed in binding assays may be different from those in functional assays because of differences in assay conditions

TABLE 3

Summary of parameters from ligand cross-competition. All the values were obtained in 50 mM Tris-HCl, pH 7.4, at 22°C. Cross-competition were carried out in filter binding assays by varying concentrations of both competition partners with radioligand set at a constant level, and the data were fit to eq. 3 for homologous cross-competition or eq. 4 for heterologous cross-competition by nonlinear squares analysis to calculate $K_{i(1)}$, the inhibition constant for partner one (I_1), $K_{i(2)}$, the inhibition constant for I_2, and γ , the cooperativity factor for the interaction between I_1 and I_2.

Competition Pair		γ	$K_{i(1)}$	$K_{i(2)}$
I_1	I_2			
			nM	*nM*
SPA with ^{125}I-[MePhe^7]NKB as the radioligand				
[MePhe^7]NKB	Talnetant	>100	0.7 ± 0.1	4.4 ± 0.8
[MePhe^7]NKB	Osanetant	>100	0.5 ± 0.1	0.6 ± 0.1
Talnetant	Osanetant	>100	3.1 ± 0.2	0.6 ± 0.1
Filter binding with [^{3}H]SB222200 as the radioligand				
SB222200	Talnetant	70	1.26 ± 0.13	1.95 ± 0.19
SB222200	Osanetant	>100	1.10 ± 0.10	0.21 ± 0.02
Talnetant	Osanetant	>100	2.00 ± 0.21	0.20 ± 0.02

such as pH, temperature, ionic strength, viscosity, etc. Thus, a molecule displaying normal kinetic properties in binding may behave in a different way in functional assays as a result of the changes in assay conditions, leading to nonequilibrium conditions in the functional assays. If this were indeed the case, longer preincubation of cells with osanetant would have improved the abnormal Schild. The fact that the aberrant Schild observed for osanetant remains unchanged by longer preincubation (Fig. 4B) argues against the idea of inadequate equilibration as the reason for the steep Schild slope in the cell-based Ca^{2+} mobilization assay.

Potential time effects may also be evaluated using Schild incorporating a time-component according to eq. 16 (Kenakin, 1980). This temporal Schild equation assumes that the equilibration is not diffusion-controlled but rather is limited by antagonist-receptor interaction. Allowing this time-component would, in principle, lead to improved estimate of the true K_b value for steep Schild plot if indeed the onset of antagonism is slow. Although analysis by applying this temporal equation can adequately describe the "steep" Schild plot for osanetant (Fig. 4C), in this case, it seems to overestimate the potency of osanetant, yielding K_b values of 8, 4, and 10 pM, respectively, for 10-, 30-, or 55-min preincubation, values much less than the IC_{50} of 0.8 nM from competition binding or the K_i of 0.2 to 0.6 nM (Table 3) from ligand cross-competition.

Second, it is conceivable that the abnormal Schild plot observed with osanetant in the Ca^{2+} mobilization assay, as described in the current investigation and in other functional assays reported previously (Emonds-Alt et al., 1995; Nguyen-Le et al., 1996; Beaujouan et al., 1997; Medhurst et al., 1997), reflects a binding mechanism different from that of talnetant. The results from kinetic (Fig. 5 and Table 2) and cross-competition binding studies (Figs. 6 and 7 and Table 3) are consistent with osanetant and talnetant binding in a similar one-step binding mechanism at the same site, a site within the orthosteric binding domain, arguing against a mechanism of binding as the reason for the observed aberrant Schild.

However, these data from kinetic and cross-competition studies are not in themselves conclusive evidence. Homology modeling based on the high-resolution X-ray crystal structure of rhodopsin has been used to provide insights into the ligand binding sites of all three neurokinin receptors (Giolitti

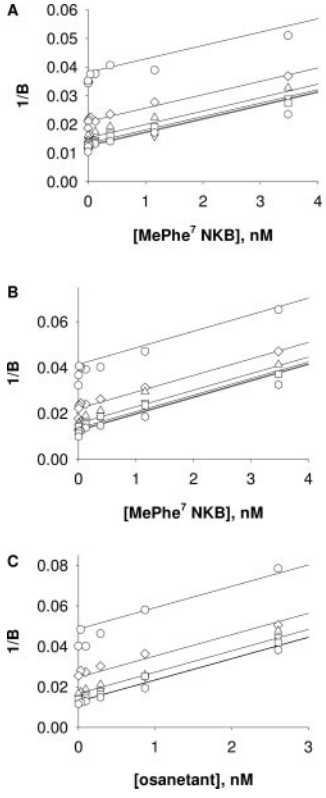

Fig. 6. Radioligand cross-competition with ^{125}I-[MePhe^7]NKB by talnetant and osanetant. Radioligand cross-competition with ^{125}I-[MePhe^7]NKB as the radioligand was carried out in 50 mM Tris-HCl, pH 7.4, at 22°C as described under *Materials and Methods*. Reciprocal of bound ligand (1/*B*) was plotted against [I_1] at various [I_2] to determine the mode of homologous ligand cross-competition between [MePhe^7]NKB and talnetant (A), with [talnetant] set at 0 (hexagon), 0.22 (□), 0.65 (▽), 2.0 (△), 5.9 (◇), and 17.6 (○) nM, and between [MePhe^7]NKB and osanetant (B), with [osanetant] set at 0 (hexagon), 0.032 (□), 0.097 (▽), 0.29 (△), 0.87 (◇), and 2.6 (○) nM, or heterologous ligand cross-competition between osanetant and talnetant (C), with [talnetant] set at 0 (hexagon), 0.22 (□), 0.65 (▽), 2.0 (△), 5.9 (◇), and 17.6 (○) nM. In all cases, the slope did not change with [I_2], indicating competitive ligand cross-competition.

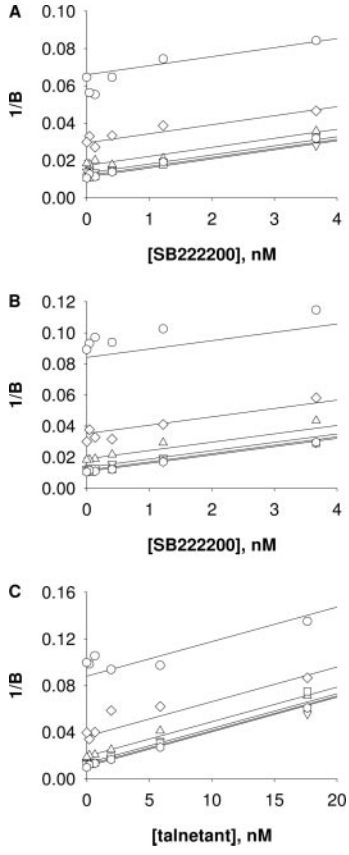

Fig. 7. Radioligand cross-competition with [^{3}H]SB222200 by talnetant and osanetant. Radioligand cross-competition with [^{3}H]SB222200 as the radioligand was carried out in 50 mM Tris-HCl, pH 7.4, at 22°C as described under *Materials and Methods*. Reciprocal of bound ligand (1/*B*) was plotted against [I_1] at various [I_2] to determine the mode of homologous ligand cross-competition between SB222200 and talnetant (A), with [talnetant] set at 0 (hexagon), 0.22 (□), 0.65 (▽), 2.0 (△), 5.9 (◇), and 17.6 (○) nM, and between SB222200 and osanetant (B), with [osanetant] set at 0 (hexagon), 0.032 (□), 0.097 (▽), 0.29 (△), 0.87 (◇), and 2.6 (○) nM, or heterologous ligand cross-competition between talnetant and osanetant (C), with [osanetant] set at 0 (hexagon), 0.032 (□), 0.097 (▽), 0.29 (△), 0.87 (◇), and 2.6 (○) nM. In all cases, the slope did not change with [I_2], indicating competitive binding.

et al., 2000; Blaney et al., 2001; Pieper et al., 2002) and in conjunction with site-directed mutagenesis and pharmacophore analysis (Evers and Klebe, 2004; Meini et al., 2004) to help understand the nature of the interactions between neurokinin receptors and antagonists. Although a homology model of NK_3 docked with talnetant has been described previously (Blaney et al., 2001), pharmacophore modeling using shape similarity or point-matching did not identify sufficient common pharmacophore features between talnetant and osanetant (C. Alhambra, unpublished data), suggesting low probability for binding of talnetant and osanetant at the same site on the receptor through an identical set of interactions. This pharmacophore analysis does not rule out the possibility that the two antagonists bind to the same pocket on the receptor via different sets of interactions or have partially overlapping binding sites on the receptor. Both scenarios are consistent with the observed competitive ligand cross-competition while allowing room for differential functional effects to arise from distinct interactions of the two antagonists occupying their respective partially overlapping sites. To unequivocally demonstrate overlapping binding sites would require the application of a structural approach, such as X-ray crystallography or affinity labeling.

Finally, a competitive ligand in binding may not necessarily show competitive antagonism in functional assays if the coupling between binding and function can be perturbed by certain antagonists to become nonlinear and/or multiphasic. This possibility cannot be ruled out for NK_3 antagonists because little is known about the structure of the orthosteric site and quantitative nature of its interaction with the components of downstream signaling pathways.

Several features of ligand cross-competition make it an attractive mechanistic probe to investigate the mechanism of action of pharmacological compounds. This method allows the use of relatively low concentrations of radioligand, thereby circumventing the limitation for Schild type analysis whenever high-background radioligand binding is a problem. In addition, ligand cross-competition allows one to evaluate the mode of action of different compounds (for example, novel leads identified by various screening approaches) without having to radiolabel the compounds themselves (assuming a radiolabeled orthosteric ligand is available). Although designed primarily to investigate modes of action between multiple drug molecules, the mechanism of binding of a drug molecule with regard to orthosteric ligand can be readily determined through homologous ligand cross-competition. Perhaps most importantly, cross-competition studies can be performed with ligands that have affinity too weak for use as radioligands. Thus, ligand cross-competition analysis can be used to determine whether two weak affinity novel lead compounds are competitive with one another and therefore whether overlapping structure-activity relationships should be anticipated, because structural changes are designed into the leads during optimization toward higher-affinity compounds. Finally, this method is not limited to binding assays; in cases in which the coupling between binding and function is linear or their relationship can be analytically defined, one should be able to use ligand cross-competition to investigate the mechanism of interaction between two drug molecules in functional assays.

Appendix: Derivation of Equation 1 for Ligand Cross-Competition

The total amount of bound radioligand is defined by the following equation:

$$B = S([\mathrm{RA}] + [\mathrm{RAI_1}] + [\mathrm{RAI_2}] + [\mathrm{RAI_1I_2}]) \quad (17)$$

where S is the specific activity of the radioligand. Given that the dissociation and inhibition constants as well as the cooperativity factors to describe the binding equilibria involved in eq. 1 in the text are defined as follows:

$$K_\mathrm{d} = \frac{[\mathrm{A}][\mathrm{R}]}{[\mathrm{RA}]} \quad (18)$$

$$K_{\mathrm{i}(1)} = \frac{[\mathrm{I_1}][\mathrm{R}]}{[\mathrm{RI_1}]} \quad (19)$$

$$K_{\mathrm{i}(2)} = \frac{[\mathrm{I_2}][\mathrm{R}]}{[\mathrm{RI_2}]} \quad (20)$$

$$\alpha K_{\mathrm{i}(1)} = \frac{[\mathrm{I_1}][\mathrm{RA}]}{[\mathrm{RAI_1}]} \quad (21)$$

$$\beta K_{\mathrm{i}(2)} = \frac{[\mathrm{I_2}][\mathrm{RA}]}{[\mathrm{RAI_2}]} \quad (22)$$

$$\gamma K_{\mathrm{i}(1)} = \frac{[\mathrm{I_1}][\mathrm{RI_2}]}{[\mathrm{RI_1I_2}]} \quad (23)$$

$$\delta\alpha K_{\mathrm{i}(1)} = \frac{[\mathrm{I_1}][\mathrm{RAI_2}]}{[\mathrm{RAI_1I_2}]} \quad (24)$$

and that the mass balance is given by

$$R_\mathrm{t} = [\mathrm{R}] + [\mathrm{RA}] + [\mathrm{RAI_1}] + [\mathrm{RAI_2}] + [\mathrm{RAI_1I_2}] + [\mathrm{RI_1}] + [\mathrm{RI_2}] + [\mathrm{RI_1I_2}] \quad (25)$$

it can be demonstrated that

$$[\mathrm{RA}] = \frac{R_\mathrm{t}\dfrac{[\mathrm{A}]}{K_\mathrm{d} + [\mathrm{A}]}}{1 + \left(\dfrac{\alpha K_\mathrm{d} + [\mathrm{A}]}{K_\mathrm{d} + [\mathrm{A}]}\right)\dfrac{[\mathrm{I_1}]}{\alpha K_{\mathrm{i}(1)}} + \left(\dfrac{\beta K_\mathrm{d} + [\mathrm{A}]}{K_\mathrm{d} + [\mathrm{A}]}\right)\dfrac{[\mathrm{I_2}]}{\beta K_{\mathrm{i}(2)}} + \left(\dfrac{(\alpha\beta\delta/\gamma)K_\mathrm{d} + [\mathrm{A}]}{K_\mathrm{d} + [\mathrm{A}]}\right)\dfrac{[\mathrm{I_1}][\mathrm{I_2}]}{\alpha\beta\delta K_{\mathrm{i}(1)}K_{\mathrm{i}(2)}}} \quad (26)$$

$$[\mathrm{RAI_1}] = [\mathrm{RA}]\frac{[\mathrm{I_1}]}{\alpha K_{\mathrm{i}(1)}} \quad (27)$$

$$[\mathrm{RAI_2}] = [\mathrm{RA}]\frac{[\mathrm{I_2}]}{\beta K_{\mathrm{i}(2)}} \quad (28)$$

and

$$[\mathrm{RAI_1I_2}] = [\mathrm{RA}]\left(\frac{1}{\delta}\right)\left(\frac{[\mathrm{I_1}]}{\alpha K_{\mathrm{i}(1)}}\right)\left(\frac{[\mathrm{I_2}]}{\beta K_{\mathrm{i}(2)}}\right) \quad (29)$$

Substituting eqs. 25 to 29 in eq 17 and defining B_max as SR_t, we arrive at the following equation:

$$B = \frac{B_{max}\frac{[A]}{K_d + [A]}\left(1 + \frac{[I_1]}{\alpha K_{i(1)}} + \frac{[I_2]}{\beta K_{i(2)}} + \frac{[I_1][I_2]}{\alpha\beta\delta K_{i(1)}K_{i(2)}}\right)}{1 + \left(\frac{\alpha K_d + [A]}{K_d + [A]}\right)\frac{[I_1]}{\alpha K_{i(1)}} + \left(\frac{\beta K_d + [A]}{K_d + [A]}\right)\frac{[I_2]}{\beta K_{i(2)}} + \left(\frac{(\alpha\beta\delta/\gamma)K_d + [A]}{K_d + [A]}\right)\frac{[I_1][I_2]}{\alpha\beta\delta K_{i(1)}K_{i(2)}}} \quad (30)$$

which is eq. 1 in the text.

Acknowledgments

We thank Lois Lazor for establishing initial conditions for radioligand binding assays, Dr. Cristobal Alhambra for sharing results from pharmacophore modeling of talnetant and osanetant, and Dr. David Aharony for useful comments regarding this manuscript.

References

Albert JS (2004) Neurokinin antagonists and their potential role in treating depression and other stress disorders. *Expert Opin Ther Pat* **14:**1421–1433.

Almeida TA, Rojo J, Nieto PM, Pinto FM, Hemandez M, Martin JD, and Candenas ML (2004) Tachykinins and tachykinin receptors: structure and activity relationships. *Curr Med Chem* **11:**2045–2081.

Beaujouan JC, Saffroy M, Torrens Y, and Glowinski J (1997) Potency and selectivity of the tachykinin NK3 receptor antagonist SR 142801. *Eur J Pharmacol* **319:**307–316.

Blaney FE, Raveglia LF, Artico M, Cavagnera S, Dartois C, Farina C, Grugni M, Gagliardi S, Luttmann MA, Martinelli M, et al. (2001) Stepwise modulation of neurokinin-3 and neurokinin-2 receptor affinity and selectivity in quinoline tachykinin receptor antagonists. *J Med Chem* **44:**1675–1689.

Emonds-Alt X, Bichon D, Ducoux JP, Heaulme M, Miloux B, Poncelet M, Proietto V, Van Broeck D, Vilain P, Neliat G, et al. (1995) SR 142801, the first potent non-peptide antagonist of the tachykinin NK3 receptor. *J Life Sci* **56:**PL27–PL32.

Evers A and Klebe G (2004) Successful virtual screening for a submicromolar antagonist of the neurokinin-1 receptor based on a ligand-supported homology model. *J Med Chem* **47:**5381–5392.

Gerspacher M (2005) Selective and combined neurokinin receptor antagonists. *Prog Med Chem* **43:**49–103.

Giardina GAM, Raveglia LF, Grugni M, Sarau HM, Farina C, Medhurst AD, Graziani D, Schmidt DB, Rigolio R, Luttmann MA, et al. (1999) Discovery of a novel class of selective non-peptide antagonists for the human neurokinin-3 receptor. 2. Identification of (S)-N-(1-phenylpropyl)-3-hydroxy-2- phenylquinoline-4-carboxamide (SB 223412). *J Med Chem* **42:**1053–1065.

Giolitti A, Cucchi P, Renzetti AR, Rotondaro L, Zappitelli S, and Maggi CA (2000) Molecular determinants of peptide and nonpeptide NK-2 antagonists binding sites of the human tachykinin NK-2 receptor by site-directed mutagenesis. *Neuropharmacology* **39:**1422–1429.

Holmes A, Heilig M, Rupniak NM, Steckler T, and Griebel G (2003) Neuropeptide systems as novel therapeutic targets for depression and anxiety disorders. *Nat Rev Drug Dis* **24:**580–588.

Kenakin TP (1980) Effects of equilibration time on the attainment of equilibrium between antagonists and drug receptors. *Eur J Pharmacol* **66:**295–306.

Knappenberger KS, Tian G, Ye X, Sobotka-Briner C, Ghanekar SV, Greenberg BD, and Scott CW (2004) Mechanism of γ-secretase cleavage activation. Is γ-secretase regulated through autoinhibition involving the presenilin-1 exon 9 loop. *Biochemistry* **43:**6208–6218.

Kronenberg G, Berger P, Tauber RF, Bandelow B, Henkel V, and Heuser I (2005) Randomized, double-blind study of SR142801 (Osanetant). A novel neurokinin-3 (NK3) receptor antagonist in panic disorder with pre- and posttreatment cholecystokinin tetrapeptide (CCK-4) challenges. *Pharmacopsychiatry* **38:**24–29.

Lutz M and Kenakin T (1999) *Quantitative Molecular Pharmacology and Informatics in Drug Discovery*. John Wiley & Sons, England.

Medhurst AD, Parsons AA, Roberts JC, and Hay DWP (1997) Characterization of NK3 receptors in rabbit isolated iris sphincter muscle. *Br J Pharmacol* **120:**93–101.

Meini S, Bellucci F, Catalani C, Cucchi P, Patacchini R, Rotondaro L, Altamura M, Giuliani S, Giolitti A, and Maggi CA (2004) Mutagenesis at the human tachykinin NK_2 receptor to define the binding site of a novel class of antagonists. *Eur J Pharmacol* **448:**61–69.

Nguyen-Le XK, Nguyen QT, Pheng LH, Emonds-Alt X, Breliere JC, and Fregoli D (1996) Pharmacological characterization of SR 142801: a new non-peptide antagonist of the neurokinin-3 receptor. *Pharmacology* **52:**283–291.

Pieper U, Eswar N, Stuart AC, Ilyin VA, and Sali A (2002) MODBASE, a database of annotated comparative protein structure models. *Nucleic Acids Res* **30:**255–259.

Sarau HM, Griswold DE, Bush B, Potts W, Sandhu P, Lundberg D, Foley JJ, Schmidt DB, Webb EF, Martin DL, et al. (2000) Nonpeptide tachykinin receptor antagonists. II. Pharmacological and pharmacokinetic profile of SB-222200, a central nervous system penetrant, potent and selective NK-3 receptor antagonist. *J Pharmacol Exp Ther* **295:**373–381.

Sarau HM, Griswold DE, Potts W, Foley JJ, Schmidt DB, Webb EF, Martin DL, Brawner ME, Elshourbagy NA, Medhurst AD, et al. (1997) Nonpeptide tachykinin receptor antagonists: I. Pharmacological and pharmacokinetic characterization of SB 223412, a novel, potent and selective neurokinin-3 receptor antagonist. *J Pharmacol Exp Ther* **281:**1303–1311.

Spooren W, Riemer C, and Meltzer H (2005) Opinion - NK3 receptor antagonists: the next generation of antipsychotics. *Nat Rev Drug Dis* **4:**967–975.

Tian G, Ghanekar SV, Aharony D, Shenvi AB, Jacobs RT, Liu X, and Greenberg BD (2003) The mechanism of γ-secretase: multiple inhibitor binding sites for transition state analogs and small molecule inhibitors. *J Biol Chem* **278:**28968–28975.

Address correspondence to: Dr. Gaochao Tian, AstraZeneca Pharmaceuticals, 1800 Concord Pike, Wilmington, DE 19803. E-mail: gaochao.tian@astrazeneca.com